Dalton Transactions

Synthesis and Bonding Analysis of Pentagonal Bipyramidal Rhenium Carboxamide Oxo Complexes

Journal:	*Dalton Transactions*
Manuscript ID	DT-ART-08-2023-002617.R1
Article Type:	Paper
Date Submitted by the Author:	28-Sep-2023
Complete List of Authors:	McMillion, Noah D; The University of North Carolina at Chapel Hill Bruch, Quinton; Massachusetts Institute of Technology, Chemistry Chen, Chun-Hsing; University of North Carolina at Chapel Hill Hasanayn, Faraj; American University of Beirut, Chemistry Miller, Alexander; University of North Carolina at Chapel Hill, Department of Chemistry

Synthesis and Bonding Analysis of Pentagonal Bipyramidal Rhenium Carboxamide Oxo Complexes

Noah D. McMillion[†], Quinton J. Bruch[†], Chun-Hsing Chen[†], Faraj Hasanayn[‡,], and Alexander J. M. Miller[†,*]*

[†] Department of Chemistry, University of North Carolina at Chapel Hill, Chapel Hill, North Carolina 27599-3290, United States

[‡] Department of Chemistry, American University of Beirut, Beirut 1107 2020, Lebanon

* Corresponding author information: F.H. (fh19@aub.edu.lb); A.J.M.M. (ajmm@email.unc.edu)

ORCID

Noah D. McMillion: 0000-0002-6221-9935

Quinton J. Bruch: 0000-0002-3653-1036

Chen-Hsing Chen: 0000-0003-0150-9557

Faraj Hasanayn: 0000-0003-3308-7854

Alexander J. M. Miller: 0000-0001-9390-3951

Seven-coordinate rhenium oxo complexes supported by a tetradentate bipyridine carboxamide/carboxamidate ligand are reported. The neutral dicarboxamide H_2^{Ph}bpy-da ligand initially coordinates in an L_4 (ONNO) fashion to an octahedral rhenium oxo precursor, yielding a seven-coordinate rhenium oxo complex. Subsequent deprotonation generates a new oxo complex featuring the dianionic (L_2X_2) carboxamidate (NNNN) form of the ligand. Computational studies provide insight into the relative stability of possible linkage isomers upon deprotonation. Structural

studies and molecular orbital theory are employed to rationalize the relative isomer stability and provide insight into the rhenium-oxo bonding order.

Introduction

Carboxamides and their conjugate bases, carboxamidates, act as ligands in a diverse array of coordination chemistry. Carboxamides bind most commonly through the carbonyl oxygen atom but can also bind through the amide N in either tautomer (Figure 1A).[1–3] The conjugate base carboxamidates can bind through oxygen or nitrogen as well (Figure 1A).[4] Both ligands can also support additional interactions such as hydrogen bonding.[4–8] Carboxamide and carboxamidate complexes have seen use in catalytic water oxidation and hydroamination of unsaturated carbon-carbon bonds, among other transformations.[5,9–14] In addition, carboxamide and carboxamidate ligands have applications in medicinal chemistry, for example as radiopharmaceutical tracers or anticancer agents.[1,15–19]

Our interest in applying tridentate, pincer-ligated rhenium complexes to N_2 fixation chemistry led us to consider tetradentate ligands as an alternative motif to avoid the formation of multiple isomeric N_2 complexes.[20,21] The ligand 6,6'-bis(phenylcarbamoyl)-2,2'-bipyridine (H_2^{Ph}bpy-da)[22] in particular attracted our attention for exploring novel rhenium coordination chemistry that might eventually be applied to nitrogen fixation.[23] Approaching the synthesis, we recognized the possibility that several binding modes (NNNN, ONNN, or ONNO) could be accessible due to the rotational freedom of the pendent carboxamidate moieties (Figure 1B). Such linkage isomerism is frequently encountered in carboxamidate ligands, with different isomers being observed when pH, steric bulk, oxidation state, and metal identity are varied.[4,8,15,19] Additional structural complexity could arise from access to either six- or seven-coordinate complexes. The wide bite angle of tetradentate ligands derived from bipyridine can enable binding

of a fifth ligand in the plane of the ligand, as seen in ruthenium complexes featuring a dicarboxylate analog to $[^{Ph}bpy\text{-}da]^{2-}$.[24]

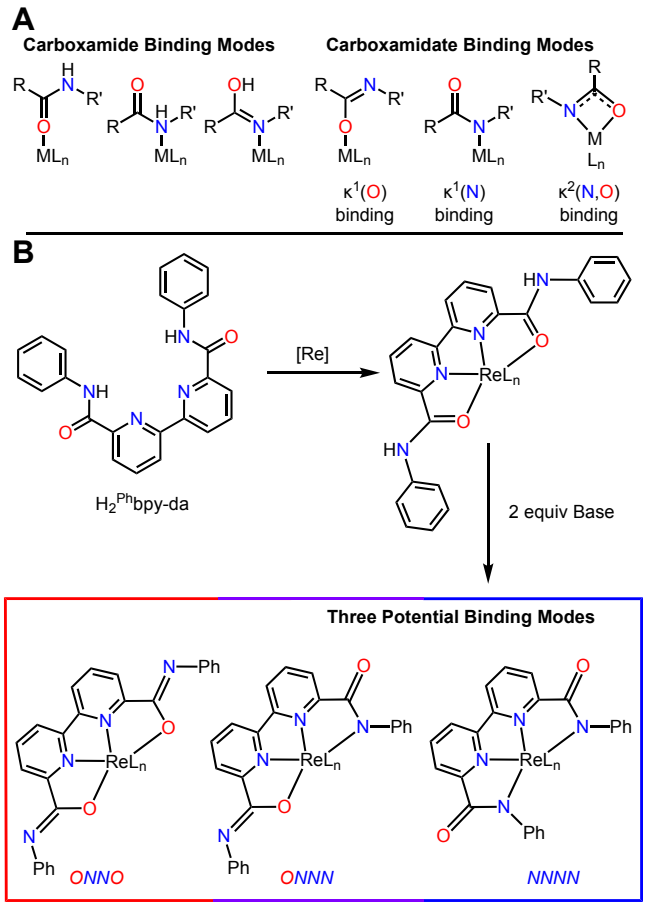

Fig. 1 (A) Binding modes of carboxamide and carboxamidate ligands. (B) Metalation of dicarboxamide ligand $H_2{}^{Ph}bpy\text{-}da$ highlighting possible linkage isomers for its doubly deprotonated analogue.

Here, we report the rhenium coordination chemistry of $H_2{}^{Ph}bpy\text{-}da$ and its deprotonated analogue, $[^{Ph}bpy\text{-}da]^{2-}$. $H_2{}^{Ph}bpy\text{-}da$ coordinates to a Re^{V} center as an L_4 ligand to yield a seven-coordinate pentagonal bipyramidal metal oxo complex $[Re(H_2{}^{Ph}bpy\text{-}da)(O)(Cl)_2]^+$ ($[\mathbf{1}]^+$). Subsequent deprotonation produces an anionic pentagonal bipyramidal metal oxo complex $[Re(^{Ph}bpy\text{-}da)(O)(Cl)_2]^-$ ($[\mathbf{2}]^-$) and crystallographic and computational studies provide insight into

the most stable ligand binding mode. Qualitative molecular orbital analyses are used to describe bonding in the rhenium-oxo bond and explain the origin of the strong oxo *trans* influence in the pentagonal plane.

Results and discussion

Synthesis and characterization

The neutral ligand H_2^{Ph}bpy-da was prepared via a two-step synthetic procedure similar to that reported by Llobet and coworkers.[22] Carboxamidate metal complexes are typically prepared either by deprotonation of the carboxamide moieties before addition to a metal precursor or by mixing a metal precursor and ligand in the presence of base.[22,25–27] To replicate these conditions, H_2^{Ph}bpy-da was allowed to react with various rhenium precursors including K_2ReCl_6, $Re(O)(OEt)(I)_2(PPh_3)_2$, $Re(Me_2S)(OPPh_3)(O)(Cl)_3$, $Re(N)(Cl)_2(PPh_3)_2$, and $ReCl_5$ in the presence of either $NaN(SiMe_3)_2$ or NEt_3.[28,29] Unfortunately, these reactions all yielded intractable mixtures.

An alternative metallation route was pursued in which H_2^{Ph}bpy-da was added to metal precursors in the absence of base. Treating the previously reported Re^V precursor, $Re(Me_2S)(OPPh_3)(O)(Cl)_3$ with H_2^{Ph}bpy-da and $NaBAr^F{}_4$ (Ar^F = 3,5-bis(trifluoromethyl)phenyl) resulted in a color change from seafoam green to crimson (Scheme 1).[28] Workup of the reaction mixture enabled isolation of a crimson product, [**1**][$BAr^F{}_4$], in 32% yield, which displayed an amide N-*H* proton at 10.26 ppm in CD_3CN (10.13 in the free ligand, Figure S5). The solid-state structure was determined for the related hexafluorophosphate salt, which proved more crystalline. Diffraction of crystals grown from NH_4PF_6-saturated MeCN at –30 ºC confirmed the structure as the seven-coordinate rhenium oxo complex *trans*-[$Re(H_2^{Ph}$bpy-da$)(O)(Cl)_2]^+$ (Figure 2B).

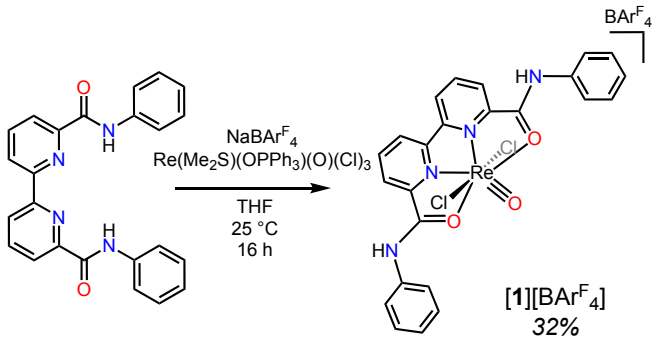

Scheme 1 Synthesis of [**1**][BAr$^F_4$].

Only a few crystallographically characterized seven-coordinate rhenium oxos have been reported.[30–33] This unusual coordination number is likely to be enabled in the present system due to the three 5-membered metallocycles formed upon coordination of H_2^{Ph}bpy-da to a larger rhenium ion, leaving ample room in the H_2^{Ph}bpy-da plane for a fifth ligand due to a wide O1-Re1-O3 angle of 155.35(8)º. Every atom of the carboxamide ligand in [**1**][PF_6] sits in the same plane (Figure 2A). A *trans* geometry is adopted in which the oxo sits in the pentagonal plane. The measured Re1–O2 distance in [**1**][PF_6] is 1.683(2) Å, which is close to the average distance of 1.692 Å (σ = 0.029 Å) for other pentagonal bipyramidal Re^V terminal oxo complexes (Table S10) as well as the average distance of 1.682 Å (σ = 0.015 Å) for octahedral Re^V terminal oxo complexes containing a bipyridine ligand (Table S11). The amide C–O bond distances are 1.248(3) Å and 1.255(3) Å, slightly longer than those seen crystallographically for the free ligand, 1.226(2) Å. The structure of the free ligand as well as the structure of [**1**][PF_6] both reveal a solid state preference for the phenyl groups to be *trans* to the pyridine ring, presumably minimizing steric interactions between aromatic groups. The average Re–N(bpy) distances in [**1**][PF_6] is 2.295 Å. This distance was compared to Re–N(bpy) distances in octahedral Re^V terminal oxo complexes, where the bond distance is affected by the geometric relationship of the pyridine unit to the oxo ligand (Table S11). For these previously reported complexes, the average Re–N(bpy) bond

distance is 2.159 Å (σ = 0.044) for the pyridine *cis* to the oxo and the average Re–N(bpy) bond distance is 2.282 Å (σ = 0.034) for the pyridine *trans* to the oxo. It is striking that pentagonal bipyramidal [**1**][PF_6] has *two* Re–N(bpy) distances that are *both* similar to Re–N(bpy) distances when the pyridine unit is *trans* to the oxo in an octahedral geometry, even though the oxo is not positioned directly across from either N atom. The origin of this strong *trans* influence will be discussed below.

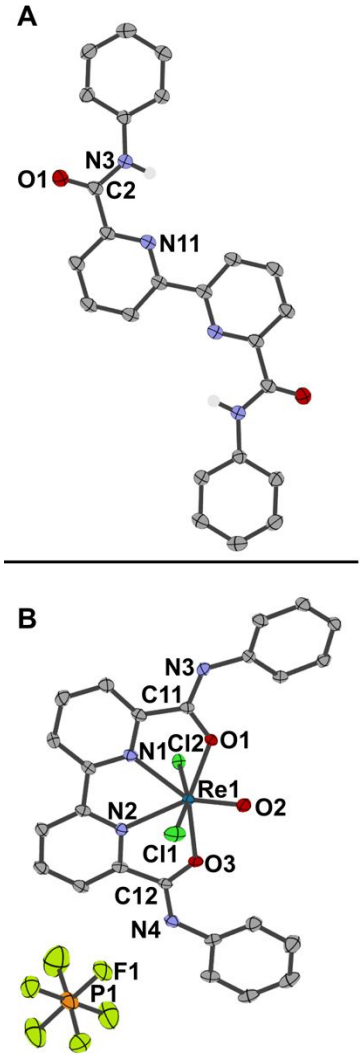

Fig. 2 (A) X-ray structure of H_2^{Ph}bpy-da (50% probability ellipsoids, hydrogen atoms omitted for clarity except for N-H protons). Distances (Å): C2-N3: 1.352(1), C2-O1: 1.226(2). (B): X-ray

structure of [**1**][PF_6] (50% probability ellipsoids, hydrogen atoms omitted for clarity). Distances (Å) and angles (º): Re1–N1 2.302(2), Re1–N2 2.287(2), Re1–O1 2.129(2), Re1–O2 1.683(2), Re1–O3 2.132(2), Re1-Cl1 2.3479(7), Re1-Cl2 2.3564(6), C11-N3 1.329(3), C12-N4 1.335(3), C11-O1 1.255(3), C12-O3 1.248(3). O1–Re1–O2 77.45(9), O2–Re1–O3 77.97(9), O3–Re1–N2 68.59(8), N2–Re1–N1 67.42(8), N1–Re1–O1 68.57(8), Cl1–Re1–Cl2 162.50(2). See Supporting Information (SI) for complete list of bond lengths (Table S2 for H_2^{Ph}bpy-da, Table S5 for [**1**][BAr^F_4]) and angles (Table S3 for H_2^{Ph}bpy-da, Table S6 for [**1**][BAr^F_4]).

With [**1**]$^+$ in hand, deprotonation of the carboxamide ligand to access the carboxamidate complex was attempted. Since an ONNO binding mode was observed in [**1**]$^+$, it seemed plausible that an oxophilic Re(V) center might retain coordination mode after deprotonation. However, the rotational freedom of the carboxamide-bipyridine C-C bond made it impossible to rule out a change in connectivity to NNNN. Adding 2.3 equivalents of NEt^{i}Pr$_2$ to a crimson solution of [**1**][BAr^F_4] in MeCN gradually yielded a dark orange solution within 30 minutes (Scheme 2). ^{1}H NMR and IR spectra both indicated that complete deprotonation of carboxamide N-*H* protons had occurred. ESI-MS corroborated double deprotonation, since the positive mode fragment [Re(H_2^{Ph}bpy-da)(O)(Cl)]$^+$ ([**1**]$^+$, *m/z* 667.0288) was no longer detected, and a negative mode ion that was two mass units lighter appeared instead, consistent with [Re(^{Ph}bpy-da)(O)(Cl)$_2$]$^-$ ([**2**]$^-$, *m/z* 665.0153). The [HNEt^{i}Pr$_2$]$^+$ countercation could be replaced by treatment with excess $NaBAr^F_4$ to yield [Na][**2**] in 51% yield. The salt [Na][**2**] was poorly soluble in all tested solvents, facilitating purification of the complex while inhibiting attempts at characterization. Treating [Na][**2**] with aza-18-crown-6 (a18c6) or 18-crown-6 improved the solubility in acetonitrile, and in the case of a18c6 also enabled growth of orange single crystals by vapor diffusion of Et_2O into a concentrated acetonitrile solution of [Na•a18c6][**2**] at -30 ºC (Figure 3A).

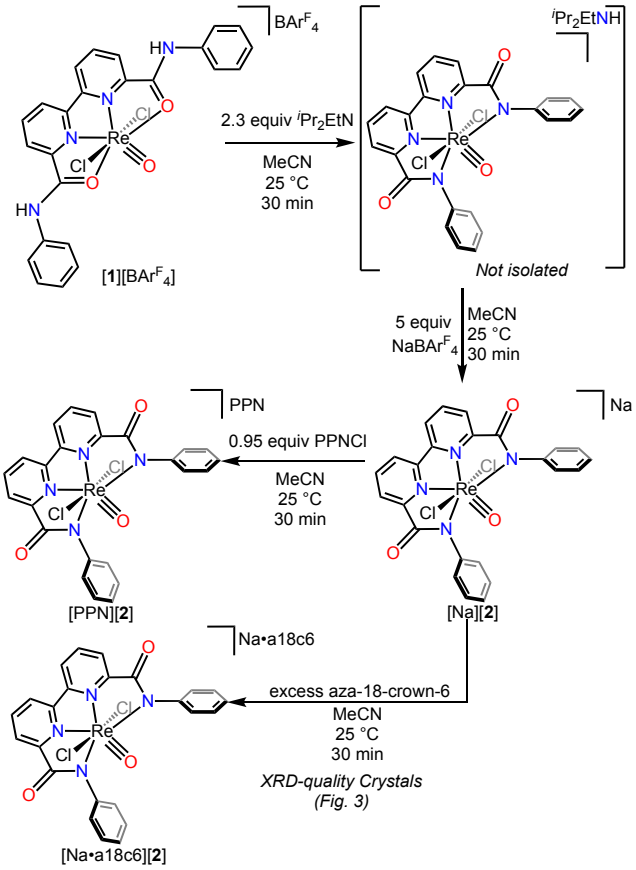

Scheme 2 Deprotonation of [**1**][BAr$^F_4$] to yield [Na][**2**] and subsequent conversion to [PPN][**2**] or [Na•a18c6][**2**].

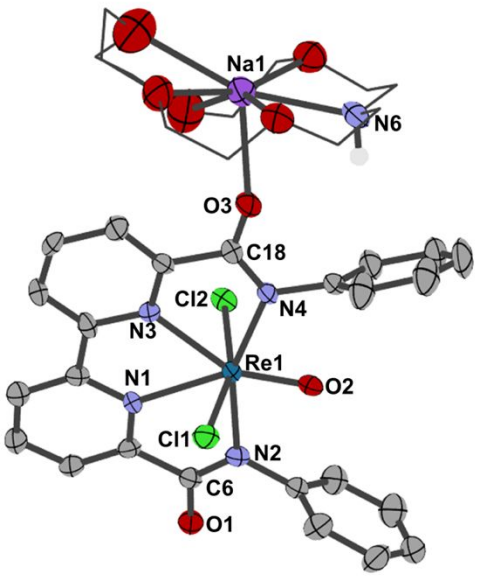

Fig. 3 X-ray structure of [Na•a18c6][**2**]. Two molecules of MeCN and all hydrogen atoms except for the one attached to N6 have been omitted for clarity, carbon atoms of a18c6 are shown in wireframe, and thermal ellipsoids are shown at 50% probability. Distances (Å) and angles (º): Re1–N1 2.319(7), Re1–N2 2.229(7), Re1–N3 2.305(8), Re1–N4 2.212(7), Re1–O2 1.687(6), Re1-Cl1 2.386(2), Re-Cl2 2.368(2), C18-N4 1.33(1), C6-N2 1.32(1), C18–O3 1.25(1), C6–O1 1.25(1), Na1-O3 2.388(8), N6–O3 2.99(1), N2–Re1–O2 78.6(3), O2–Re1–N4 78.4(3), N4–Re1–N3 68.6(2), N3–Re1–N1 66.6(2), N1–Re1–N2 67.9(2). See SI for complete list of bond lengths (Table S8) and angles (Table S9).

The solid-state structure of [Na•a18c6][**2**] features $[^{Ph}bpy\text{-}da]^{2-}$ bound in an NNNN fashion, with $[Na•a18c6]^{+}$ coordinated to one of the $[^{Ph}bpy\text{-}da]^{2-}$ carboxamidates. Deprotonation of [**1**][PF_6] therefore must be accompanied by rotation about the C–C bond connecting the bipyridine and the carboxamidate moieties switch from O-binding in $[\mathbf{1}]^{+}$ to N-binding in $[\mathbf{2}]^{-}$. In contrast to the structure of [**1**][BAr^F_4], the ligand phenyl substituents are rotated nearly perpendicular to the bipyridine-carboxamidate plane in [Na•a18c6][**2**]. As with [**1**][PF_6] and other reported pentagonal bipyramidal Re^V oxo complexes, the oxygen atom remains in the pentagonal plane in [Na•a18c6][**2**]. The Re≡O bond length in [Na•a18c6][**2**] is 1.687(6) Å, essentially the same as that in [**1**][PF_6], and the average Re–N(bpy) bond distance in [Na•a18c6][**2**] is 2.312 Å, approximately 0.02 Å greater than in [**1**][PF_6]. Finally, the amine nitrogen of a18c6 is positioned proximal to the carboxamidate oxygen (N6-O3 = 2.99(1) Å, N–H–O angle of 110.42 º). This could possibly indicate that the carboxamide oxygen engages in both dative bonding with Na^+ and hydrogen bonding with the macrocyclic ammine.[34]

Another cation exchange was performed with the more soluble bis(triphenylphosphine)iminium (PPN^+) ion by treating [Na][**2**] with [PPN][Cl] in MeCN to give

[PPN][**2**] in 88% yield. [PPN][**2**] also facilitated studies to determine the reversibility of the structural changes occurring during the deprotonation of the coordinated H_2^{Ph}bpy-da ligand. We were especially interested in this process given that 5d transition metals are often substitutionally inert.[35–37] To assess the reversibility of this change, [PPN][**2**] was treated with two equivalents of $[H(OEt_2)_2][BAr^F{}_4]$ at room temperature (Scheme 3). This resulted in reformation of [**1**][$BAr^F{}_4$] in greater than 95% yield within one hour according to ^{1}H NMR spectroscopy (Figure S13). These results suggest that there is not a significant kinetic barrier associated with the change in binding mode when the ligand protonation state is changed.

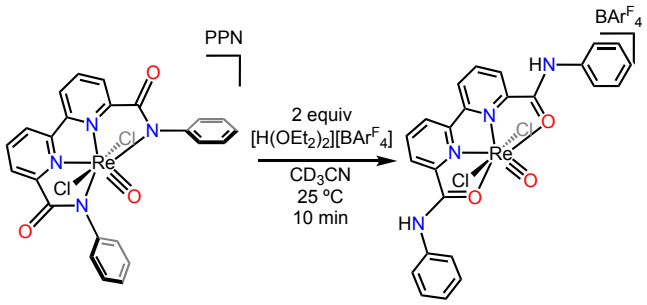

Scheme 3 Treatment of [PPN][**2**] with 2 equivalents of $[H(OEt_2)_2][BAr^F{}_4]$ to regenerate [**1**][$BAr^F{}_4$].

DFT studies of possible linkage isomers

Dicarboxamidate ligands such as [^{Ph}bpy-da]$^{2-}$ can conceivably bind either through oxygen or nitrogen given the rotational freedom of the C–C bond between the carboxamidate and bipyridine backbone.[19,38–40] To understand the energetic landscape connecting the different linkage isomers, density functional theory (DFT) calculations were undertaken, and the results are summarized in Figure 4. Consistent with the crystallographically determined structure of [**2**]$^-$, the calculations predict the NNNN coordination mode to be more favorable than the ONNO or ONNN modes. However, the computed energy differences among the three isomers are not substantial, varying within 3.3 kcal/mol.

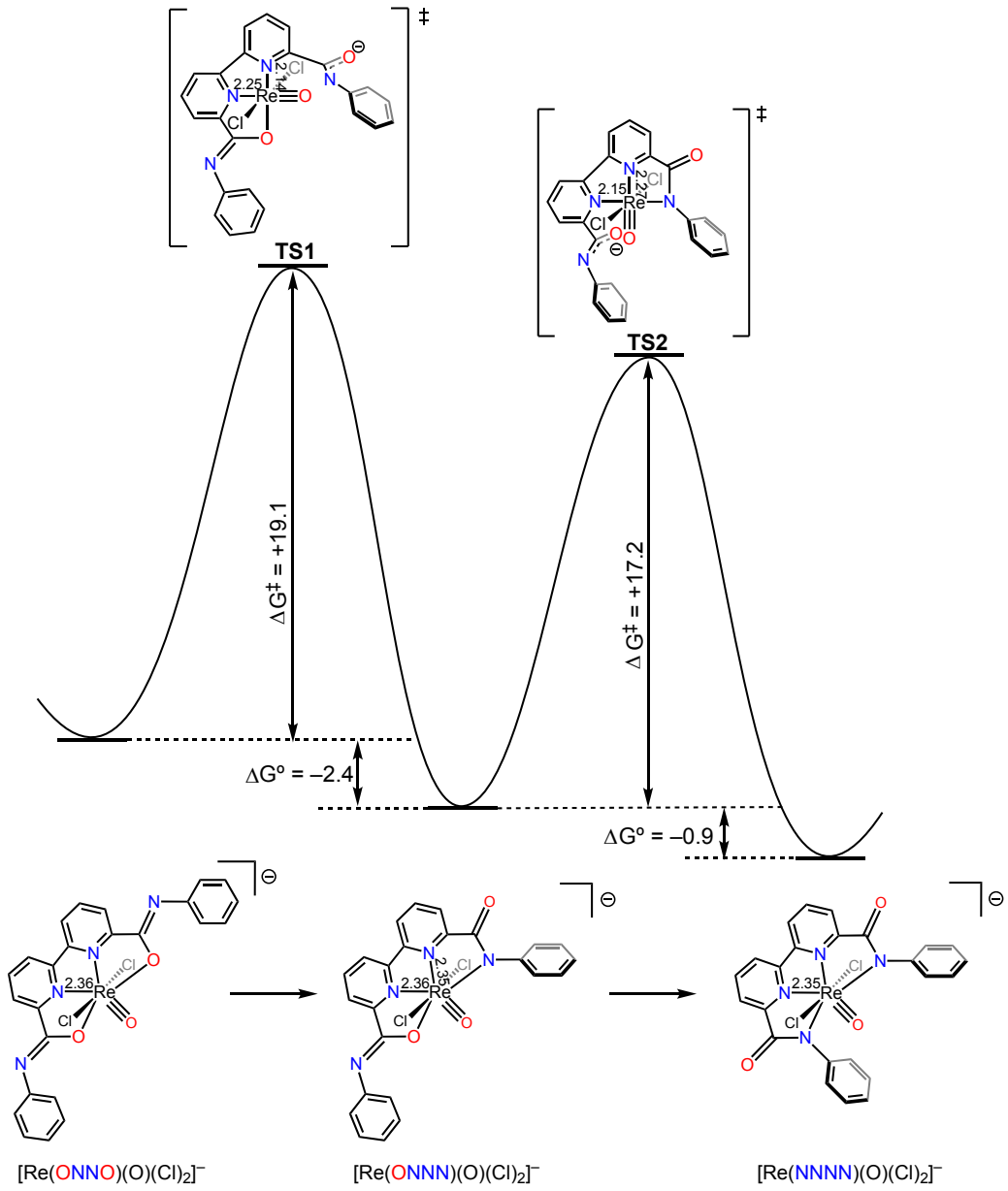

Fig. 4 Computed Gibbs free energies and selected bond distances for linkage isomers in [**2**]$^{-}$ and the transition states (**TS1** and **TS2**) for their interconversion. M06L results in THF continuum in kcal/mol at 298 K and 1 M; bond distances in Å.

The barrier to linkage isomerization was also examined computationally. The transition state structures for interconversion between ONNO and ONNN binding (**TS1**) and for the interconversion between ONNN and NNNN binding (**TS2**) feature rotation of the carboxamidate moiety by 90º from the bpy plane, implying complete dissociation of one ligand in the transition state. Nevertheless, isomerization barriers are computed to be low, 19.1 and 17.2 kcal/mol, for **TS1** and **TS2** respectively. This probably follows from a stabilizing structural reorganization into a pseudo-octahedral geometry in which the Re-N(bpy) bonds are significantly contracted compared to the respective bonds in the pentagonal bipyramidal reactants and products. For example, $[Re(ONNO)(O)(Cl)_2]^-$ (i.e. the product of double deprotonation of $[\mathbf{1}]^+$) has computed Re-N(bpy) distances of 2.36 Å; in **TS1** these bonds become inequivalent, with bond distances of 2.14 and 2.25 Å for the positions *cis* and *trans* to the oxo, respectively.

A plausible mechanism for the formation of NNNN-bound $[\mathbf{2}]^-$ starts with deprotonation of the ONNO-bound complex $[\mathbf{1}]^+$, followed by isomerization to the ONNN and then NNNN complex. By the principle of microscopic reversibility, formation of $[\mathbf{1}]^+$ from $[\mathbf{2}]^-$ would occur by a linkage isomerization/protonation mechanism. The low computed barriers for the latter isomerizations via **TS2** and **TS1** (18.1 and 21.5 kcal/mol, respectively, Figure 4) imply kinetically facile isomerization that is consistent with the experimentally observed rapid reversion of $[\mathbf{2}]^-$ to $[\mathbf{1}]^+$ upon addition of acid.

Bonding in pentagonal bipyramidal rhenium oxo complexes

Monometallic rhenium oxo complexes with a pentagonal bipyramidal geometry are rare, and warrants further study to understand bonding in these complexes.[30–33] The crystallographic and computed geometries of $[\mathbf{1}]^+$ and $[\mathbf{2}]^-$ are distinguished by a short rhenium-oxo bond as well as long Re-N(bpy) distances. Qualitative molecular orbital diagrams shown in Figure 5 suggest

these features result from triple bond character in the Re≡O unit. Figure 5 starts with the MO diagram of a D_{5h} pentagonal bipyramid, adopting an axis convention with the z-axis in the pentagonal plane in preparation for a descent in symmetry to the C_{2v} structures of interest. Next, σ- and π- antibonding interactions of the oxo, chloride, and $H_2{}^{Ph}$bpy-da/[^{Ph}bpy-da]$^{2-}$ ligands were incorporated. The d_{yz} and d_{xz} orbitals are significantly destabilized by the strong π-donor oxygen, while the d_{xy} orbital is expected to be only mildly destabilized by the Cl π-donors. Thus, the lowest energy MO with predominantly d-orbital character is d_{xy}, and this is expected to be occupied by the two d-electrons in a low-spin $S = 0$ d^2 configuration. This fits with the experimental spectroscopic data, given that the complexes are diamagnetic. DFT computations based on [**2**]$^-$ (but simplified by replacement of N–Ph with N–H) produced MOs that have the same character and energy ordering as in the qualitative MO diagram. This configuration leaves the MOs with ReO π* character empty, so the Re≡O unit can be assigned a bond order of 3. The Re–oxo bond length in crystal structures of both [**1**]$^+$ and [**2**]$^-$ is consistent with other Re–oxo bonds assigned the same bond order in pseudooctahedral environments featuring bipyridine-based supporting ligands (Table S11). A filled d_{xy} orbital and a Re-oxo triple bond formulation would also be expected for pseudooctahedral complexes. It is worth noting that the orbital ordering may be influenced by the specific supporting ligands employed or structural distortions.

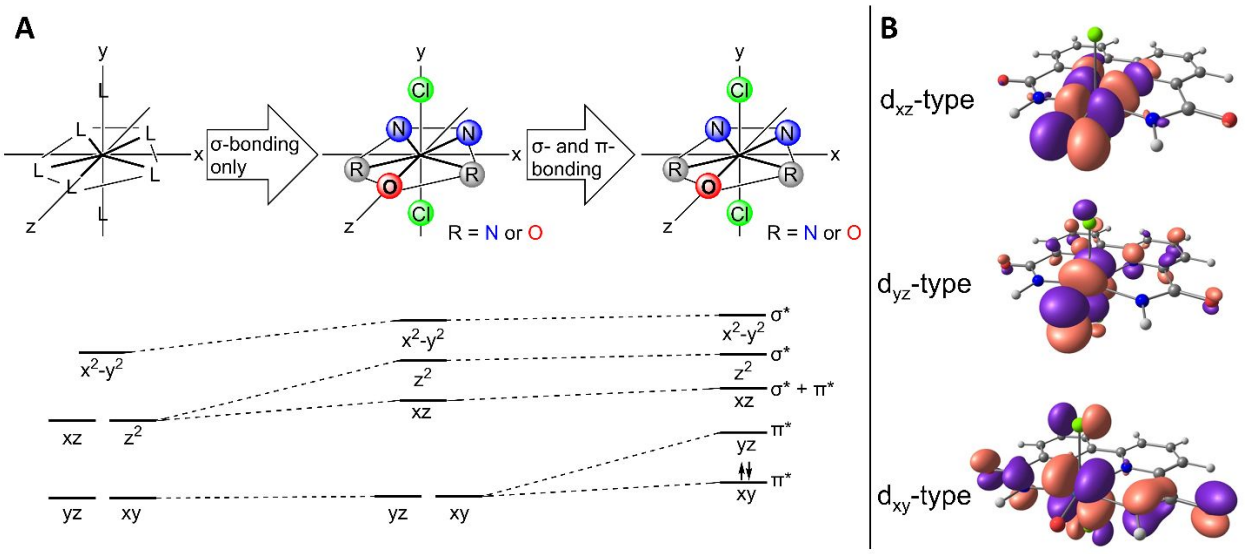

Fig. 5 A: Constructing a qualitative MO diagram for [**1**]$^{+}$ and [**2**]$^{-}$ to assign ReO bond order. B: Canonical orbital renderings of MOs with largest Re d_{xz}, Re d_{yz}, and Re d_{xy} character. MOs rendered with isosurface value of 0.3 e Å^{-3}.

The d_{xz} symmetry MO has both Re≡O π* character and Re–N(bpy) σ* antibonding character, revealing an interesting feature of σ/π mixing when the oxo is situated in the pentagonal plane. The O lone pairs and bpy N lone pairs are both donating to the same d-orbital, enabling a strong oxo *trans* influence that leads to long Re–N(bpy) bond lengths (Figure S30). The *trans* influence of the oxo can also be seen in linkage isomerism transition states, where one pyridine unit is *trans* to a carboxamidate donor and the other is *trans* to the oxo. The Re–N(bpy) bond length is always calculated to be significantly longer when *trans* to the oxo.

Conclusions

We report the synthesis of two new pentagonal bipyramidal rhenium oxo complexes supported by planar tetradentate dicarboxamide and dicarboxamidate ligands. Coordination of the

neutral bipyridine dicarboxamide to rhenium formed one oxo complex in an ONNO binding mode; deprotonation and linkage isomerization generated another NNNN-bound complex. These studies provide a procedural framework for synthesis of other metal carboxamide and carboxamidate complexes in this geometry.

Structural and computational studies confirm that nitrogen is the thermodynamically preferred anionic donor for rhenium in this system. A qualitative molecular orbital bonding picture was developed for the relatively rare pentagonal bipyramidal geometry, providing an intuitive framework which could be applied in the reported complexes to assign a rhenium-oxygen triple bond. Computational methods support the validity of the qualitative model while providing insight into the cooperative effects of an unusually strong oxo ligand *trans* influence and weaker bipyridine donors in imparting stability to these seven-coordinate complexes.

Experimental Section

General Considerations

All manipulations, except those to synthesize H_2^{Ph}bpy-da, were carried out under an N_2 atmosphere using standard glovebox and Schlenk techniques. Under standard glovebox operating conditions pentane, diethyl ether (Et_2O), benzene, toluene, tetrahydrofuran (THF), were used without purging, such that traces of each solvent were present in the atmosphere and in the solvent bottles during manipulations. Acetonitrile (MeCN) and dichloromethane (CH_2Cl_2) were purged from the atmosphere after use. Unless otherwise stated, reagents used were commercial and used without further purification. $Re(OPPh_3)(Me_2S)(O)(Cl)_3$ was synthesized in accordance with literature methods.[41] $NaBAr^F_4$ was obtained commercially or synthesized and recrystallized using literature methods.[42,43] ^1H and $^{13}C\{^1H\}$ NMR spectra were recorded on 400 or 600 MHz

spectrometers at 298 K in the University of North Carolina's Department of Chemistry NMR Core Laboratory. Deuterated solvents for NMR were purchased from Cambridge Isotopes Laboratories, Inc. ^{1}H and ^{13}C chemical shifts are reported relative to residual proteo solvent resonances. High-resolution mass spectrometery (HRMS) was performed in the University of North Carolina's Department of Chemistry Mass Spectrometry Core Laboratory on a Q Exactive HF-X (ThermoFischer, Bremen, Germany) mass spectrometer. Samples were introduced via a microelectrospray source at a flow rate of 3 μL/min. XCalibur (ThermoFischer, Bremen, Germany) was used to analyze the data. Solution-phase infrared spectroscopy was carried out with a Thermo Scientific Nicolet iS5 FT-IR in MeCN. Single-crystal X-ray diffraction (XRD) data were collected on a Bruker APEX-II CCD diffractometer with Cu Kα radiation (λ = 1.54175 Å). Diffraction studies of H_2^{Ph}bpy-da and [**1**][PF_6] were performed at 150 K; [Na•a18c6][**2**] was collected at 293 K. See supporting information for individual details on each crystal structure. Elemental analysis was performed at Robertson Microlit Laboratories (Ledgewood, NJ).

6,6'-diphenylcarboxamido-2,2'-bipyridine (H_2^{Ph}bpy-da)

H_2^{Ph}bpy-da was synthesized via a preparation similar to that reported by Llobet and coworkers, and spectra of the ligand collected for this work matched reported spectra reasonably well.[22] A 50 mL round bottom flask was charged with a stir bar, 2,2'-bipyridine-6,6'-dicarboxylic acid (400.3 mg, 1.639 mmol), dimethylformamide (0.1 mL), and $SOCl_2$ (6.0 mL). The resulting slurry was vigorously stirred and became homogeneous while refluxing for 4 hours under N_2. The yellow reaction solution was dried *in vacuo* to give a yellow-white powder that was subsequently suspended in 15 mL of dry toluene. Triethylamine (0.45 mL, 3.23 mmol) was added dropwise, and the solution was stirred for 2 minutes. Aniline (0.30 mL, 3.29 mmol) was then added dropwise, yielding a tan suspension which was stirred for 16 hours. This suspension was filtered, and the

solids were washed with 200 mL EtOH and 200 mL pentane to give an off-white solid that was dried overnight under vacuum to give 503.4 mg 6,6'-diphenylcarboxamido-2,2'-bipyridine (79% yield). **^{1}H NMR** (CD_3CN, 8% CD_2Cl_2, 600 MHz): δ 10.13 (br s, 2H, N*H*), 8.94 (dd, 2H, 3,3'-bpy(C*H*), *J* = 7.9, 1.1 Hz), 8.34 (dd, bpy-5,5', 2H, *J* = 7.7, 1.1 Hz), 8.21 (t, 2H, bpy-4,4', *J* = 7.8 Hz), 7.88 (d, 4H, *ortho*-NC_6H_5, *J* = 7.6 Hz), 7.44 (t, 4H, *meta*-NC_6H_5, *J* = 7.6 Hz), 7.20 (tt, 2H, *para*-NC_6H_5, *J* = 7.4 Hz, 1.1 Hz). **^{13}C{^{1}H} NMR** (CD_3CN 8% CD_2Cl_2, 151 MHz): δ 161.23 (s, *C*=O), 152.82 (s, bpy), 148.86 (s, bpy), 138.33 (s, bpy-4,4'), 137.22 (s, *ipso*-N*C*$_6$H$_5$), 128.09 (s, *meta*-N*C*$_6$H$_5$), 123.59 (s, bpy-3,3'), 123.50 (s, *para*-N*C*$_6$H$_5$), 122.04 (s, bpy-5,5'), 119.51 (s, *ortho*-N*C*$_6$H$_5$). **IR:** ν_{CO} 1688 cm^{-1}.

[Re(bpy-da)(Cl)$_2$(O)][BAr$^F_4$] ([1][BAr$^F_4$])

In an N_2-filled glovebox, a 20 mL scintillation vial was charged with a stir bar, H_2^{Ph}bpy-da (250.0 mg, 0.6338 mmol), $NaBAr^F_4$ (561.6 mg, 0.6337 mmol), and $Re(O)(OPPh_3)(Me_2S)(Cl)_3$ (411.3 mg, 0.6342 mmol), and 5 mL of THF. This mixture was allowed to stir for 16 hours at room temperature, during which a color change from seafoam green to deep crimson was observed. The reaction mixture was first filtered and then concentrated by half *in vacuo*. The crimson solution was then added to 10 mL of vigorously stirring pentane to flocculate a sticky scarlet solid. This solid was isolated via vacuum filtration before extracting it into Et_2O. This Et_2O solution was taken to dryness *in vacuo* to yield a mixture of [**1**][BAr^F_4], H_2^{Ph}bpy-da, and triphenylphosphine oxide as a sticky solid. Attempts to remove unreacted ligand and triphenylphosphine oxide by recrystallization, solvent washes, or continuous liquid-liquid extraction were unsuccessful. Instead, this mixture was removed from the glovebox atmosphere and dissolved in 10 mL of acetonitrile under air. The resulting deep red acetonitrile solution was then extracted sixty times in a separatory funnel with 50 mL of hexanes. Over the course of ten of these extractions, the product

precipitated as a deep red residue on the sides of the separatory funnel. Poor phase separation also resulted in some oil containing [**1**][BAr^F_4] passing through the separatory funnel and ending up in the hexanes fraction. Therefore, the hexanes fraction was decanted from the oil and discarded before adding an additional 10 mL of MeCN to redissolve both the product-containing oil and residue. Hexanes extractions were then resumed. After extraction, the residue was redissolved once more in acetonitrile, filtered, and the solvent removed *in vacuo*. This procedure yielded [**1**][BAr^F_4] as a deep red sticky solid (32% yield). To obtain diffraction quality crystals of [**1**]$^+$, the mixture of [**1**][BAr^F_4], $H_2{}^{Ph}$bpy-da, and triphenylphosphine oxide obtained prior to the hexanes extractions was dissolved in a minimal volume of a saturated [NH_4][PF_6] solution in MeCN, filtered and placed in a -30 °C freezer overnight. This procedure yielded red needles of [**1**][PF_6] in low yield. **^{1}H NMR** (CD_3CN, 600 MHz): δ 10.26 (br s, 2H, N*H*), 8.58 (t, bpy-4,4', 2H, *J* = 7.9 Hz), 8.52 (dd, 2H, bpy-3,3', *J* = 8.0, 1.1 Hz), 8.45 (dd, 2H, bpy-5,5', *J* = 7.9 Hz, 1.0 Hz), 7.77 (d, 4H, *ortho*-NC_6H_5, *J* = 7.7 Hz), 7.60 (t, 4H, *meta*-NC_6H_5, *J* = 7.7 Hz), 7.42 (tt, 2H, *para*-NC_6H_5, *J* = 7.4 Hz, 1.1 Hz). **^{13}C{^{1}H} NMR** (CD_3CN, 151 MHz): δ 160.41 (s, *C*=O), 150.60 (s, bpy), 143.59 (s, bpy), 142.62 (s, bpy-4,4'), 133.26 (s, *ipso*-NC_6H_5), 128.69 (s, *meta*-NC_6H_5) 127.76 (s, bpy-3,3'), 127.39 (s, *para*-NC_6H_5), 126.55 (s, bpy-5,5'), 121.86 (s, *ortho*-NC_6H_5). **IR:** ν_{CO} 1636 cm^{-1}. **HRMS:** (ESI$^+$) *m/z* [Re(O)$(Cl)_2(H_2{}^{Ph}$bpy-da)]$^+$ calcd. for $C_{24}H_{18}N_4O_3Cl_2Re$, 667.0314; found 667.0288. **Anal. Calcd** for $C_{24}H_{18}N_4O_3Cl_2Re$: C: 43.94; H: 1.98; N: 3.66. Found: C: 43.66; H: 1.95; N: 2.74.

[Na][Re(bpy-da)$(Cl)_2$O] ([Na][2])

In an N_2-filled glovebox, a 20 mL scintillation was charged with a stir bar and [**1**][BAr^F_4] (150.0 mg, 0.09799 mmol) as a dark red solution in 10 mL of MeCN. To this solution, diisopropylethylamine (34.2 μL, 0.196 mmol) was added dropwise and the solution immediately

turned dark orange and became cloudy. The vial was sealed and stirred for 30 minutes. The vial was then reopened and $NaBAr^F_4$ (434.2 mg, 0.4900 mmol) dissolved in 2 mL MeCN was added. The vial was sealed and stirred for an additional 30 minutes, during which an intense red-orange powder precipitated. This powder was collected via filtration on a sintered glass frit and washed with 5 mL MeCN, 10 mL Et_2O, and 10 mL pentane. The solid was collected to give 34.3 mg (51%) of [Na][**2**]. Spectroscopic characterization of [Na][**2**] was impeded by its low solubility. Addition of aza-18-crown-6 to a suspension of [Na][**2**] in MeCN yielded a dark orange solution, [Na•a18c6][**2**]. This solution was then filtered and X-ray quality crystals were obtained via vapor diffusion of Et_2O into this solution at -30 °C.

[Re(bpy-da)(Cl)$_2$(O)][PPN] ([PPN][2])

In an N_2-filled glovebox, a 20 mL scintillation vial was charged with a stir bar and [Na][**2**] (34.3 mg, 0.0498 mmol). [PPN][Cl] (27.2 mg, 0.0474 mmol) as a 2 mL solution of MeCN was then added. The resulting slurry was stirred for 30 minutes, during which the colorless supernatant became dark orange. The mixture was filtered before drying the filtrate *in vacuo*. 52.9 mg of a dark orange residue, [PPN][**2**], resulted. (88% yield) **^{1}H NMR** (CD_3CN, 600 MHz): δ 8.09 (t, 2H, bpy-4,4', J = 7.8 Hz), 7.97 (dd, 2H, bpy-3,3', J = 7.7 Hz, 1.3 Hz), 7.93 (dd, 2H, bpy-5,5', J = 7.8 Hz, 1.4 Hz), 7.17 (tt, 4H, *meta*-NC_6H_5, J = 7.9 Hz, 1.5 Hz), 7.02 (t, 4H, *ortho*-NC_6H_5, J = 7.5 Hz), 6.98 (tt, 2H, *para*-NC_6H_5, J = 7.4 Hz, 1.3 Hz Hz). **^{13}C{^{1}H} NMR** (CD_3CN, 151 MHz): δ 161.77 (s, *C*=O), 152.57 (s, bpy), 152.23 (s, *ipso*-NC_6H_5), 149.70 (s, bpy), 139.33 (s, bpy-4,4'), 126.74 (s, *meta*-NC_6H_5), 126.02 (s, *ortho*-NC_6H_5), 125.27 (s, bpy-3,3'), 122.83 (s, *para*-NC_6H_5), 121.20 (s, bpy-5,5'). **IR:** ν_{CO} 1626 cm^{-1}. **HRMS:** (ESI$^-$) *m/z* [Re(O)(Cl)$_2$(^{Ph}bpy-da)]$^-$ calcd. for $C_{24}H_{16}N_4O_3Cl_2Re$, 665.0157; found 665.0153. **Anal. Calcd** for $C_{24}H_{16}N_4O_3Cl_2Re$: C: 59.85; H: 3.85; N: 5.82. Found: 59.53; H: 3.77; 5.45.

Conflicts of interest

There are no conflicts to declare.

Acknowledgments

The experimental and computational work was supported through the NSF Chemical Catalysis program under grants no. CHE-1954942 and CHE-2247257. The mass spectrometry work was supported by the NSF under grant no. CHE-1726291. The NMR spectrometry work was supported by the NSF under grant no. CHE-1828183. F.H. thanks the Alwaleed Center for American Studies and Research for support, and the AUB-HPC center for computational resources.

References

1 E. Palma, J. D. G. Correia, Â. Domingos, I. Santos, R. Alberto and H. Spies, *J. Organomet. Chem.*, 2004, **689**, 4811–4819.

2 D. V. Griffiths, Y.-K. Cheong, P. Duncanson and M. Motevalli, *Dalt. Trans.*, 2011, **40**, 10215.

3 K. L. Yip, W. Y. Yu, P. M. Chan, N. Y. Zhu and C. M. Che, *J. Chem. Soc. Dalt. Trans.*, 2003, **3**, 3556–3566.

4 A. V. Lee and L. L. Schafer, *Eur. J. Inorg. Chem.*, 2007, **2007**, 2245–2255.

5 L. J. E. Stanlake and L. L. Schafer, *Organometallics*, 2009, **28**, 3990–3998.

6 J. Rebek, *Angew. Chemie Int. Ed. English*, 1990, **29**, 245–255.

7 C. B. Aakeröy, B. M. T. Scott, M. M. Smith, J. F. Urbina and J. Desper, *Inorg. Chem.*, 2009, **48**, 4052–4061.

8 D. D. Beattie, E. G. Bowes, M. W. Drover, J. A. Love and L. L. Schafer, *Angew. Chemie Int. Ed.*, 2016, **55**, 13290–13295.

9 M. K. Coggins, M.-T. Zhang, A. K. Vannucci, C. J. Dares and T. J. Meyer, *J. Am. Chem. Soc.*, 2014, **136**, 5531–4.

10 W. C. Ellis, N. D. McDaniel, S. Bernhard and T. J. Collins, *J. Am. Chem. Soc.*, 2010, **132**, 10990–10991.

11 P. Garrido-Barros, S. Grau, S. Drouet, J. Benet-Buchholz, C. Gimbert-Suriñach and A. Llobet, *ACS Catal.*, 2019, **9**, 3936–3945.

12 W. Rabten, T. Åkermark, M. D. Kärkäs, H. Chen, J. Sun, P. G. Andersson and B. Åkermark, *Dalt. Trans.*, 2016, **45**, 3272–3276.

13 Z. Zhang and L. L. Schafer, *Org. Lett.*, 2003, **5**, 4733–4736.

14 A. L. Gott, A. J. Clarke, G. J. Clarkson and P. Scott, *Organometallics*, 2007, **26**, 1729–1737.

15 E. Kimura, T. Gotoh, S. Aoki and M. Shiro, *Inorg. Chem.*, 2002, **41**, 3239–3248.

16 X. Tao, D. W. Stephan and P. K. Mascharak, *Inorg. Chem.*, 1987, **26**, 754–759.

17 M. Papachristou, I. Pirmettis, T. Siatra-Papastaikoudi, M. Pelecanou, C. Tsoukalas, C. P. Raptopoulou, A. Terzis, E. Chiotellis and M. Papadopoulos, *Eur. J. Inorg. Chem.*, 2003, **2003**, 3826–3830.

18 C. M. A. Muller, M. V. Babak, M. Kubanik, M. Hanif, S. M. F. Jamieson, C. G. Hartinger and L. J. Wright, *Inorganica Chim. Acta*, 2016, **450**, 124–130.

19 S. H. van Rijt, A. J. Hebden, T. Amaresekera, R. J. Deeth, G. J. Clarkson, S. Parsons, P. C. McGowan and P. J. Sadler, *J. Med. Chem.*, 2009, **52**, 7753–7764.

20 B. M. Lindley, R. S. Van Alten, M. Finger, F. Schendzielorz, C. Würtele, A. J. M. Miller, I. Siewert and S. Schneider, *J. Am. Chem. Soc.*, 2018, **140**, 7922–7935.

21 Q. J. Bruch, G. P. Connor, C.-H. Chen, P. L. Holland, J. M. Mayer, F. Hasanayn and A. J. M. Miller, *J. Am. Chem. Soc.*, 2019, **141**, 20198–20208.

22 M. Gil-Sepulcre, P. Garrido-Barros, J. Oldengott, I. Funes-Ardoiz, R. Bofill, X. Sala, J. Benet-Buchholz and A. Llobet, *Angew. Chemie - Int. Ed.*, 2021, **60**, 18639–18644.

23 Q. J. Bruch, G. P. Connor, N. D. McMillion, A. S. Goldman, F. Hasanayn, P. L. Holland and A. J. M. Miller, *ACS Catal.*, 2020, **10**, 10826–10846.

24 B. Zhang and L. Sun, *J. Am. Chem. Soc.*, 2019, **141**, 5565–5580.

25 A. Amiri, M. Amirnasr, S. Meghdadi, K. Mereiter, V. Ghodsi and A. Gholami, *Inorganica Chim. Acta*, 2009, **362**, 3934–3940.

26 Y. Gartia, A. Biswas, M. Stadler, U. B. Nasini and A. Ghosh, *J. Mol. Catal. A Chem.*, 2012, **363–364**, 322–327.

27 M. Ray, D. Ghosh, Z. Shirin and R. Mukherjee, *Inorg. Chem.*, 1997, **36**, 3568–3572.

28 D. E. Grove and G. Wilkinson, *J. Chem. Soc. A Inorganic, Phys. Theor.*, 1966, 1224.

29 M. Hecht, S. S. Anaya, A. Hagenbach and U. Abram, *Inorg. Chem.*, 2005, **44**, 3172–3180.

30 C. M. Che, Y. P. Wang, K. S. Yeung, K. Y. Wong and S. M. Peng, *J. Chem. Soc. Dalt. Trans.*, 1992, **524**, 2675–2677.

31 H.-Y. Jin, S. Ikari, K. Kobayashi, K. Umakoshi, H. Sugimoto, A. Mitani, M. Abe, Y. Sasaki and T. Ito, *Bull. Chem. Soc. Jpn.*, 2004, **77**, 1139–1146.

32 L. Xu, I. A. Setyawati, J. Pierreroy, M. Pink, V. G. Young, B. O. Patrick, S. J. Rettig and C. Orvig, *Inorg. Chem.*, 2000, **39**, 5958–5963.

33 M. Leeaphon, P. E. Fanwick and R. A. Walton, *Inorg. Chem.*, 1991, **30**, 4986–4995.

34 E. Arunan, G. R. Desiraju, R. A. Klein, J. Sadlej, S. Scheiner, I. Alkorta, D. C. Clary, R. H. Crabtree, J. J. Dannenber, P. Hobza, H. G. Kjaergaard, A. C. Legon, B. Mennucci and D. J. Nesbitt, *Pure Appl. Chem.*, 2011, **83**, 1637–1641.

35 P. L. Holland, *Acc. Chem. Res.*, 2015, **48**, 1696–1702.

36 K. Zhang, A. A. Gonzalez, S. L. Mukerjee, S. J. Chou, C. D. Hoff, K. A. Kubat-Martin, D. Barnhart and G. J. Kubas, *J. Am. Chem. Soc.*, 1991, **113**, 9170–9176.

37 R. Bolliger, G. Meola, H. Braband, O. Blacque, L. Siebenmann, Q. Nadeem and R. Alberto, *Inorg. Chem.*, 2020, **59**, 17600–17607.

38 J. D. Azoulay, K. Itigaki, G. Wu and G. C. Bazan, *Organometallics*, 2008, **27**, 2273–2280.

39 E. Zeini Jahromi and J. Gailer, *Dalt. Trans.*, 2010, **39**, 329–336.

40 A. K. Patra and R. Mukherjee, *Inorg. Chem.*, 1999, **38**, 1388–1393.

41 J. C. Bryan, R. E. Stenkamp, T. H. Tulip and J. M. Mayer, *Inorg. Chem.*, 1987, **26**, 2283–2288.

42 N. A. Yakelis and R. G. Bergman, *Organometallics*, 2005, **24**, 3579–3581.

43 A. J. Martínez-Martínez and A. S. Weller, *Dalt. Trans.*, 2019, **48**, 3551–3554.